Available online at www.sciencedirect.com
ScienceDirect
Trans. Nonferrous Met. Soc. China 35(2025) 715−733
Transactions of Nonferrous Metals Society of China
www.tnmsc.cn

Influence of geometric configurations on friction characteristics during incremental forming process of AA5052 sheet metal

Guang-can YANG, Da-wei ZHANG, Chong TIAN, Sheng-dun ZHAO

School of Mechanical Engineering, Xi'an Jiaotong University, Xi'an 710049, China

Received 22 July 2023; accepted 1 March 2024

Abstract: The influence of geometric configuration on the friction characteristics during incremental sheet forming of AA5052 was analyzed by integrating surface morphology and its characteristic parameters, along with plastic strain, contact pressure, and area. The interface promotes lubrication and support when wall angles were ≤ 40°, a 0.5 mm-thin sheet was used, and a 10 mm-large tool radius was employed. This mainly results in micro-plowing and plastic extrusion flow, leading to lower friction coefficient. However, when wall angles exceed 40°, significant plastic strain roughening occurs, leading to inadequate lubrication on the newly formed surface. Increased sheet thickness and decreased tool radius elevate contact pressure. These actions trigger micro-cutting and adhesion, potentially leading to localized scuffing and dimple tears, and higher friction coefficient. The friction mechanisms remain unaffected by the part's plane curve features. As the forming process progresses, abrasive wear intensifies, and surface morphology evolves unfavorably for lubrication and friction reduction.

Key words: AA5052 sheet metal; incremental forming process; geometric configurations; surface morphology characteristics; friction mechanism

1 Introduction

Incremental sheet forming (ISF) is a flexible process [1], recognized for its localized deformation and cyclic loading traits [2]. It significantly enhances the cost-effective formability of AA5052 sheet metal [3−5], addressing aerospace manufacturing needs for single and small-batch parts [6,7]. However, the substantial friction effect compromises surface quality, limiting practical industrial application [8]. Wall angle, sheet thickness, plane curve features, and tool radius in ISF are pivotal geometric parameters. Yet, the mechanism of their influence on the interface friction effect remains unclear.

Friction is pivotal in through-thickness shearing during ISF. Utilizing FEA, BAMBACH et al [9] observed this shearing and correlated its magnitude with tool dimensions and incremental step size. ALLWOOD et al [10] conducted a comprehensive study on through-thickness shearing resulting from friction in the tool movement direction, highlighting its significant contribution to enhancing the forming limit. JACKSON et al [11] investigated friction-induced displacement of upper and lower surfaces during incremental forming of sandwich panels. Notably, CHANG and CHEN [12] and YANG and CHEN [13] proposed uneven friction distribution causing circumferential twisting. Through membrane analysis, they revealed the intricate mechanism behind this twisting induced by friction. To improve friction conditions, scholars suggested innovative tools like vertical [14,15] and inclined [16] roller tools as alternatives to hemispherical tools. These tools transform sliding

Corresponding author: Da-wei ZHANG, Tel: +86-29-82668607, Fax: +86-29-82665204, E-mail: zhangdawei2000@mail.xjtu.edu.cn
DOI: https://doi.org/10.1016/S1003-6326(24)66710-5

friction into rolling friction, effectively mitigating detrimental friction effects and reducing tangential strain. This transformation substantially improves surface finish quality, emphasizing the critical role of friction effects as paramount parameters influencing ISF quality.

Several scholars evaluated the influence of geometric parameters on surface quality and extensively researched methods to enhance it, using parameters like arithmetical mean deviation of the profile (R_a) and maximum height of the profile (R_z) as characterization parameters for surface roughness [17,18]. KUMAR and GULATI [19] noted that increased sheet thickness and incremental step led to higher roughness, while increased tool radius had the opposite effect. DURANTE et al [20] corroborated these findings through AA7075 sheet incremental forming experiments and theoretical analysis, emphasizing negligible impact of forming angle on surface roughness. Moreover, MOHANTY et al [21], in Al-1100 sheet incremental forming, found an increasing trend in surface roughness with a wall angle increase from 60° to 70°. Through Taguchi experiments, KUMAR and KUMAR [22] identified sheet thickness as the most significant parameter affecting surface roughness in AA2014-T6 incremental forming, with a pronounced increase in roughness as sheet thickness increased from 1.2 to 2.3 mm. They also observed reduced roughness with a tool diameter from 16 to 18 mm but a substantial increase to 20 mm. Some studies utilized various experimental designs to investigate surface roughness at different levels of key forming parameters, determining factors influencing it and optimizing parameters for superior surface quality [23,24]. However, these studies solely focus on parameters impact on surface roughness without delving into the underlying mechanisms causing variations. Further exploration is needed to uncover the intrinsic causes of roughness variations.

Scholars focused on aligning lubrication methods and types with forming parameters for optimal effects on surface quality. In AZ31 sheet incremental forming, ZHANG et al [25] confirmed that Nano-K2Ti4O9 whiskers and organic binders enhance bond strength between the anodized lubricating coating and substrate, ensuring favorable lubrication. Similarly, XU et al [26], employing atmospheric plasma spraying, prepared nickel-coated molybdenum disulfide coatings to improve lubrication conditions, determining optimal spraying parameters for lubrication effect, surface quality, and forming force. DIABB et al [27] demonstrated that using plant oil lubrication with SiO_2 nanoparticles during AA6061 ISF induces adhesive wear, highlighting smaller tool radii's susceptibility to scratching and tearing debris, leading to increased surface roughness [28]. ŞEN et al [29] applied minimum quantity lubrication (MQL) in single-point incremental forming of 7128 sheets, improving surface roughness and morphology. LI et al [30] proposed an ISF with an interpolator between the tool and AA2024-O sheet, acting as a barrier to eliminate direct contact and sliding friction, reducing contact pressure. They noted increased surface roughness with larger tool radii and incremental steps. Despite extensive research on forming conditions' influence on surface quality, the underlying mechanisms causing variations remain incompletely elucidated.

Consequently, this study undertakes the meticulous measurement and characterization of the friction coefficients, surface morphologies and features during AA5052 parts formation, considering varying wall angles, sheet thicknesses, plane curve features, and tool radii. By combining experimental findings with tribological principles, the mechanisms behind variations in friction characteristics due to parameter changes are elucidated. This provides valuable insights into the evolution of surface quality during actual forming processes.

2 Extraction of geometric configuration and friction testing method

2.1 Extraction of geometric configuration

ISF utilizes simple and versatile tools to deform the sheet metal point by point along a predetermined process path, leading to the gradual formation of the geometric structure of the part through plastic accumulation. This technique has been successfully applied in the fabrication of aerospace components [31], automotive parts [32], and medical implants [33,34], as depicted in Fig. 1. Although various industrial parts exhibit a variety of complex geometric configurations, the plane curve features of all these configurations consist of combinations of circular arcs, straight lines, and arcs with variable curvatures. Hence, the influence

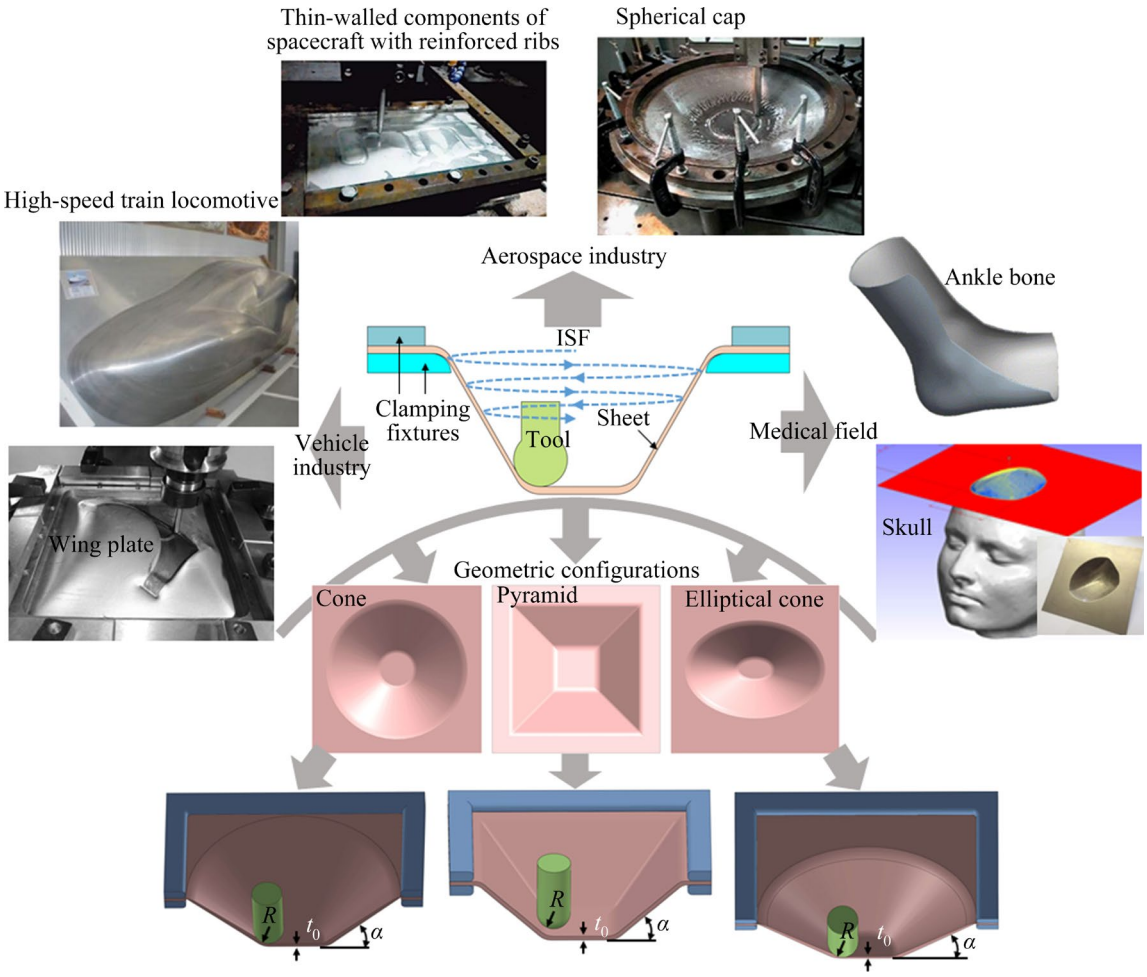

Fig. 1 Geometric configurations of parts formed by ISF

of the plane curve features on the friction characteristics in ISF can be represented by a cone part comprising a singular circular arc line, a pyramid part comprised a singular straight line, and an elliptical cone part constituted by a singular arc with variable curvature.

Furthermore, the wall angle α, sheet thickness t_0, and tool radius R are also vital parameters that determine the geometric configuration of the part. α represents the inclination angle of the part's sidewalls, exerting a significant impact on the deformation of the sheet metal and the forming force during incremental forming, thereby influencing the friction process. t_0 denotes the initial thickness of the material, which needs to be determined based on specific part requirements. It impacts the friction process in the incremental forming by altering the contact area and the forming force. R determines the minimum bending radius during the forming process. In actual production, the appropriate tool radius can be selected based on the geometric configuration of the specific part to meet the requirements. It is also essential to consider its influence on the friction process by adjusting the interface contact pressure.

2.2 Friction testing method

Friction coefficients are determined through a method proposed by our team, which establishes an equilibrium relationship between experimental and theoretical analysis forces based on the membrane analysis method to determine the friction coefficient through inverse calculation, as illustrated in Fig. 2. The experimental force refers to the average horizontal force, F_h, during the steady-state phase of ISF experimental process. The theoretical analysis force refers to the vector sum of the horizontal component of the material deformation force F_h^d and the friction force f. F_h^d includes circumferential and radial deformation forces, F_c^d

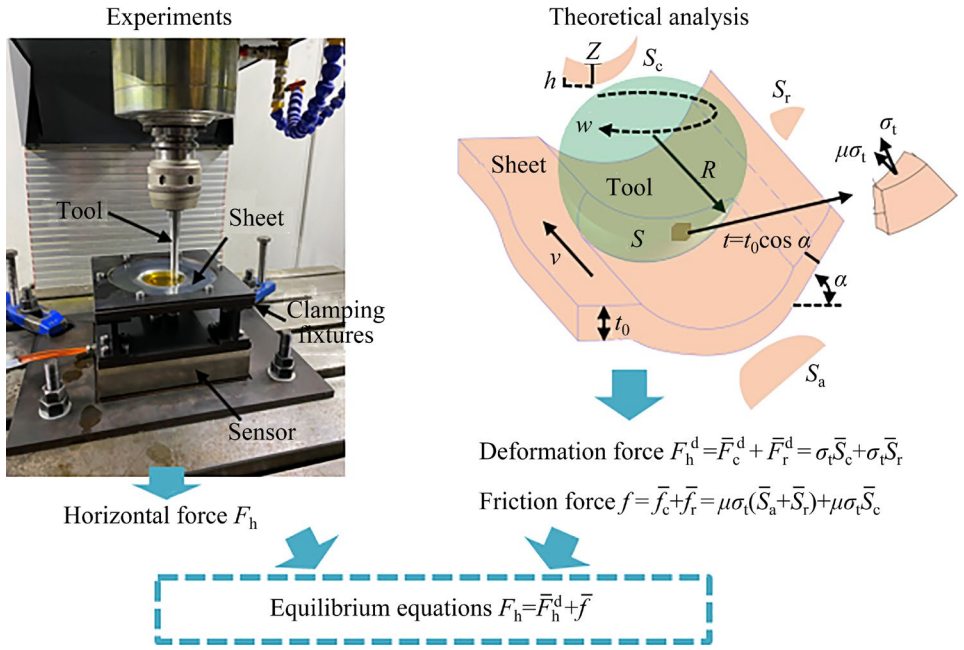

Fig. 2 Friction testing method for ISF

and F_r^d, respectively. These forces are obtained by integrating the normal stress σ_t over the projected areas S_c and S_r in the circumferential and radial directions, respectively. The friction force, f, is the vector sum of the circumferential and radial friction components, f_c and f_r, respectively. f_c acts on the axial and radial projected areas, S_a and S_r, while f_r acts on the circumferential projected area, S_c. Equation (1) can be derived as

$$F_h=\bar{F}_h^d+\bar{f}=\sqrt{\left(\sigma_t S_c+\mu\sigma_t\sqrt{S_a^2+S_r^2}\right)^2+\left(\sigma_t S_r+\mu\sigma_t S_c\right)^2} \quad (1)$$

The experimental setup depicted in Fig. 2 illustrates the apparatus utilized for acquiring the ISF process and obtaining the required F_h. The trajectory of the tool driven by the CNC machine spindle is determined based on the wall angle, plane curve features, and the step size (the amount by which the tool descends per layer) while executing ISF experiment. Sophisticated fixtures were employed to securely affix the sheet in place. Additionally, force sensors were employed to dynamically monitor the forming forces inflicted upon the sheet in real-time.

Based on the geometric relationships of the contact region shown in Fig. 2, the contact area S and its corresponding projected areas S_a, S_c and S_r can be calculated using Eq. (2):

$$\begin{aligned}S=\bar{S}_a+\bar{S}_c+\bar{S}_r=\\ &\left\{\left(\sqrt{2Rh-h^2}\left[\frac{\pi}{4}R\sin(\alpha+\arcsin\frac{Z}{2R\sin\alpha})+\sqrt{2Rh-h^2}-\frac{Z}{2\tan\alpha}\right]\right)^2+\left(\frac{1}{2}\left[(\frac{2+\pi}{2}h+R)\cdot\sqrt{2Rh-h^2}+\frac{\pi}{2}hR\sin(\alpha+\arcsin\frac{Z}{2R\sin\alpha})-R^2\cdot\arccos\frac{R-h}{R}+\frac{h^2}{\tan\alpha}\right]\right)^2+\left(\frac{\pi}{4}\sqrt{2Rh-h^2}\cdot\left[R-R\cos(\alpha+\arcsin\frac{Z}{2R\sin\alpha})-h\right]\right)^2\right\}^{1/2}\end{aligned} \quad (2)$$

h can be determined by calculating Eq. (3) [35]:

$$h=\frac{t_0(1-\cos\alpha)}{\alpha\left(3-\frac{\pi}{2}\right)+1}+\sqrt{\frac{2Zt_0}{R}} \quad (3)$$

Through the implementation of the membrane analysis method for ISF, it becomes feasible to formulate the stress equilibrium equation for the constituent contact area unit. This equation, when coupled with the Tresca yield criterion, yields a comprehensive representation of the interrelation between the stress σ_t and the material plastic stress $\sigma(\varepsilon)$, as denoted by Eq. (4):

$$\sigma_t=\frac{2t}{R+2.5t}\sigma(\varepsilon) \quad (4)$$

According to the deformation characteristics of ISF, the plastic strain ε can be calculated by [36]

$$\varepsilon=\frac{2}{\sqrt{3}}\ln\left(Rt_0\Big/\left(t\left(R+\frac{t}{2}\right)\right)\right) \tag{5}$$

Therefore, by substituting Eqs. (2)−(5) into Eq. (1), the friction coefficient μ can be obtained by

$$\mu=\left[\sqrt{\left(S_c\sqrt{S_a^2+S_r^2}+S_rS_c\right)^2+S^2\left(\frac{F_h^2}{\sigma_t^2}-S_c^2-S_r^2\right)}-(S_c\sqrt{S_a^2+S_r^2}+S_rS_c)\right]\Big/S^2 \tag{6}$$

3 Material and experimental scheme

3.1 Material

AA5052 sheet used in the experiment was rolled and annealed, with a geometric dimension of 200 mm × 200 mm. Its chemical compositions are depicted in Table 1. The stress−strain curves of this material were obtained through uniaxial tensile tests performed on an INSTRON−100 kN material testing machine, as shown in Fig. 3. It can be assumed that the material properties exhibit no significant anisotropy. Hence, the average values of the mechanical properties in the 0°, 45° and 90° directions are considered for the AA5052 sheet in the experiments. The initial surface roughness, R_a, was measured to be 0.337.

The tool material is GCr15, subjected to quenching and machining processes. The initial surface roughness, R_a, was measured to be 0.8.

Table 1 Chemical compositions of AA5052 (wt.%)

Mg	Cr	Fe	Si	Cu	Zn	Mn	Al
2.47	0.20	0.40	0.20	0.03	0.06	0.08	Bal.

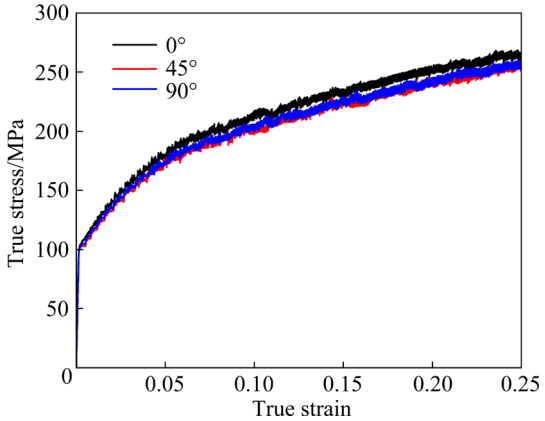

Fig. 3 True stress−true strain curves of AA5052

3.2 Experimental scheme

Considering the limitations of single-point incremental forming and the typical range of wall angles for common parts, four different wall angles, namely 30°, 40°, 50° and 60°, were chosen for forming. Five common thicknesses of AA5052 sheets, namely 0.5, 0.8, 1, 1.2 and 1.5 mm, were selected for forming. Additionally, forming experiments were conducted using tool radii of 4, 7 and 10 mm, which have significant dimensional differences. The dimensions of the various plane curve feature parts illustrated in Fig. 1 are as follows: the maximum diameter of the cone part is 70 mm, the maximum side length of the pyramid part is 100 mm, and the maximum longer and shorter axes of the elliptical cone part are 100 and 50 mm, respectively. The forming height remains consistent at 37 mm for all the parts.

A single-variable approach was employed to assess the impact of each parameter on the friction characteristics during ISF of AA5052 sheets, wherein only one parameter was varied in each experiment. The specified geometric configuration parameters used for forming the pyramid-shaped parts were a wall angle (α) of 50°, sheet thickness (t_0) of 1 mm, and a tool radius (R) of 7 mm. The specific experimental parameters are presented in Table 2. The remaining forming parameters were kept constant throughout the experiments, with a feed rate (v) of 1000 mm/min, rotation speed (w) of 500 r/min, step size (Z) of 0.5 mm, and the lubricant used was L-HM46 oil. The process path followed a spiral trajectory.

Table 2 Experimental scheme

α/(°)	t_0/mm	R/mm	Plane curve feature
30	1	7	Pyramid, cone, and elliptical cone
40	1	7	Pyramid, cone, and elliptical cone
50	1	7	Pyramid, cone, and elliptical cone
60	1	7	Pyramid, cone, and elliptical cone
50	0.5	7	Pyramid, cone, and elliptical cone
50	0.8	7	Pyramid, cone, and elliptical cone
50	1.2	7	Pyramid, cone, and elliptical cone
50	1.5	7	Pyramid, cone, and elliptical cone
50	1	4	Pyramid, cone, and elliptical cone
50	1	10	Pyramid, cone, and elliptical cone

3.3 Characterization

The influence of geometric configuration

parameters on the friction coefficient was assessed by calculating the rate of change of the friction coefficient (η) using Eq. (7), which relies on the friction coefficient (μ) at the specific forming parameters.

$$\eta=\frac{\mu-\mu_{\text{specified}}}{\mu_{\text{specified}}}\times 100\% \tag{7}$$

The surface morphology impacts the effectiveness of lubrication, the collision probability between rough peaks after lubrication film failure, and the stress levels involved. This study visually analyzed the friction traces left on the sheet surface by friction effects using SEM images at various geometric configuration parameters. The profile arithmetic mean deviation (R_a) is widely used to describe surface roughness, but it has significant limitations. Surfaces with the same R_a value can have completely different surface morphologies and performance characteristics, leading to substantial evaluation errors. To provide a more accurate description and differentiation of actual surface morphology, the skewness (R_{sk}), which reflects the asymmetry of the height distribution, and the kurtosis (R_{ku}), which reflects the peakedness of the height distribution, are further employed [37]. When $R_{sk} > 0$, the surface is predominantly concave, with minimal supporting area at the peaks, making the sharp contours susceptible to accelerated wear. On the other hand, when $R_{sk}<0$, the surface exhibits a multi-peaked profile, indicating a favorable supporting surface that facilitates wedge action to carry high loads and promote the formation of oil films. A larger R_{ku} is advantageous for reducing the real contact area and improving wear resistance. In general, a more negative R_{sk} and a larger R_{ku} are both beneficial for reducing friction.

The inner surface of the parts in contact with the tools is evenly divided into four regions: trapezoidal sides for each side with a 90° angle for the pyramid-shaped part, sector sides for every 90° along the circular direction for the cone-shaped part, and sector sides on both the major and minor axes at 90° intervals for the elliptical cone-shaped part. Only Regions 1−4 for the pyramid-shaped part are shown in Fig. 4. To represent the surface morphology throughout the entire forming process, this study divided the length of each region along the meridian direction into three equal segments. These segments were sequentially classified as the initial, intermediate, and final stages of surface formation, based on the forming sequence. In addition, surface morphology parameters were measured for each stage along both the feed direction and the meridian direction. The feed direction refers to the direction of tool movement, while the meridian direction is perpendicular to the feed direction. The surface morphology parameters along the feed and meridian directions for each stage are the average values of corresponding parameters in the four regions, which can be calculated using Eq. (8):

$$R'=\frac{R'_1+R'_2+R'_3+R'_4}{4} \tag{8}$$

where R' represents the symbol for surface morphology parameters.

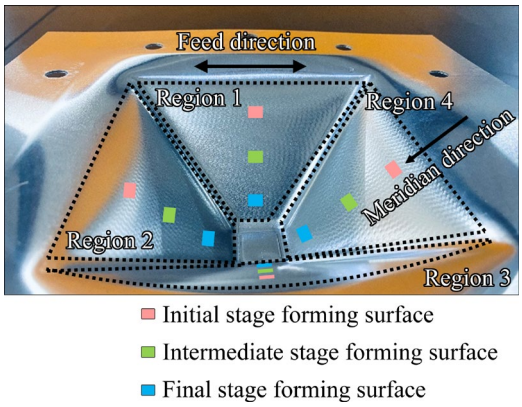

Fig. 4 Measurement regions of surface morphology

The assessment of the impact of geometric configuration parameters on surface morphology along both the feed and meridian directions during the entire formation process was carried out by examining the change rate of surface morphology parameters (λ) using Eq. (9), which is based on the specific formation parameters.

$$\lambda=\frac{R'-R'_{\text{specified}}}{R'_{\text{specified}}}\times 100\% \tag{9}$$

4 Results and discussion

4.1 Influence of wall angle

When forming cone-shaped parts with a wall angle (α) ranging from 30° to 60°, μ is 0.1003, 0.11, 0.1901 and 0.2208, respectively. In comparison to the friction coefficient at α=50°, there is a decrease of 47.238% at α=30°, a decrease of 42.136% at α=40°, and an increase of 16.149% at α=60°, as

depicted in Fig. 5(a). The change rate of μ is only 5.102% when α changes from 30° to 40°, indicating that the alteration in μ is insignificant when α is small. However, as α increases, μ exhibits a noticeable upward trend, implying a significant degradation in the interface friction condition.

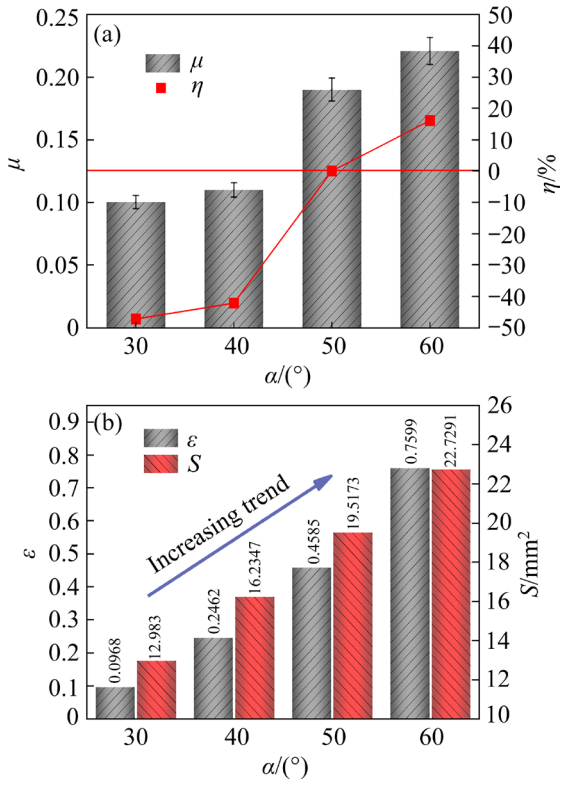

Fig. 5 Friction coefficients and their change rates (a), and plastic strain and contact area (b) at different wall angles

According to Eqs. (2) and (5), the plastic strain and contact area are calculated for $\alpha \leq 40°$, as shown in Fig. 5(b). The limited plastic strain and contact area result in insignificant plastic deformation roughening, as well as a smaller newly formed area and timely lubrication. The slight plowing action leads to relatively small and insignificant variations in R_a along the feed and meridian directions, as depicted in Figs. 6(a) and (b). Additionally, R_{sk} is relatively small and R_{ku} is large, with stable values shown in Fig. 7. Therefore, when forming small-angular parts, there is a favorable support surface and a small actual contact area, which facilitates the wedge effect in promoting the formation of oil film to bear high loads. Thus, there is mainly micro-plowing and plastic extrusion sliding during the initial stage of forming, leaving scratches on the surface, as shown in Figs. 8(a) and (b).

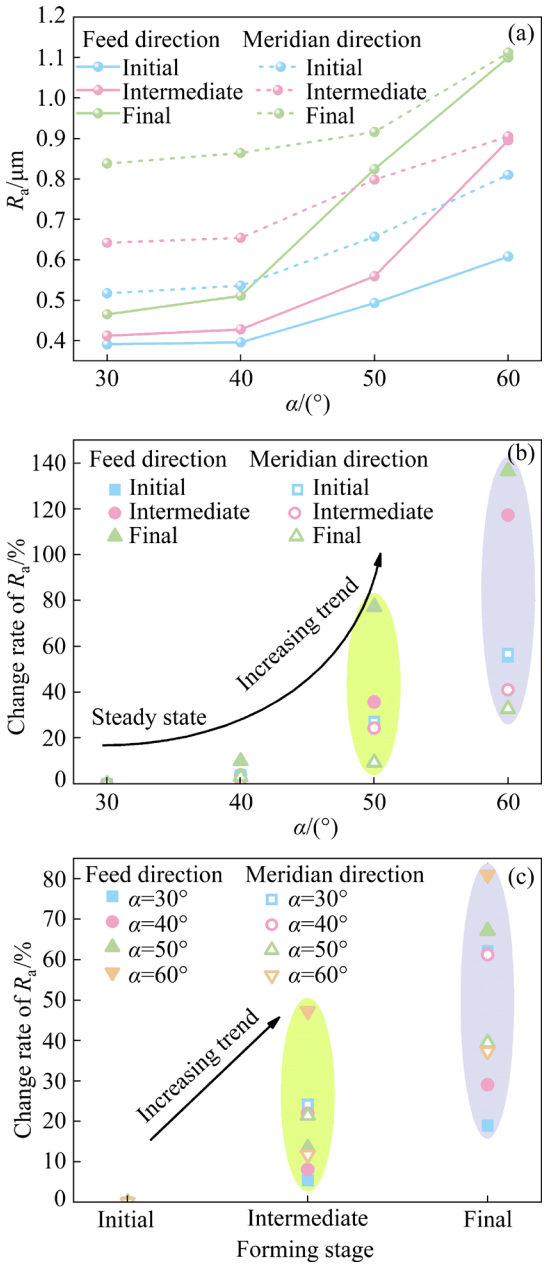

Fig. 6 R_a (a) and change rate of R_a (b) with respect to wall angle, and change rate of R_a during forming process (c)

As the forming process progresses, the accumulating debris cannot be efficiently expelled from the forming zone and enters the contact interface, resulting in an increasing trend in R_a and R_{sk}, and a decreasing trend in R_{ku}, as seen in Figs. 6(c) and 7. These effects intensify abrasive wear, leading to more surface scratches and increased depth. The material folds caused by the micro-plowing action are repeatedly extruded and piled up on the sheet surface, as shown in Figs. 8(a) and (b) during the intermediate to final stages.

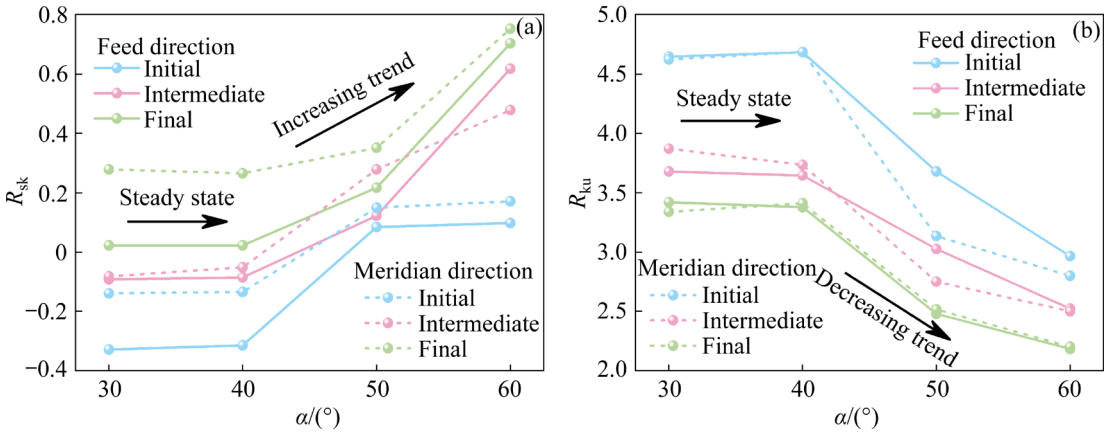

Fig. 7 R_{sk} (a) and R_{ku} (b) throughout forming process at different wall angles

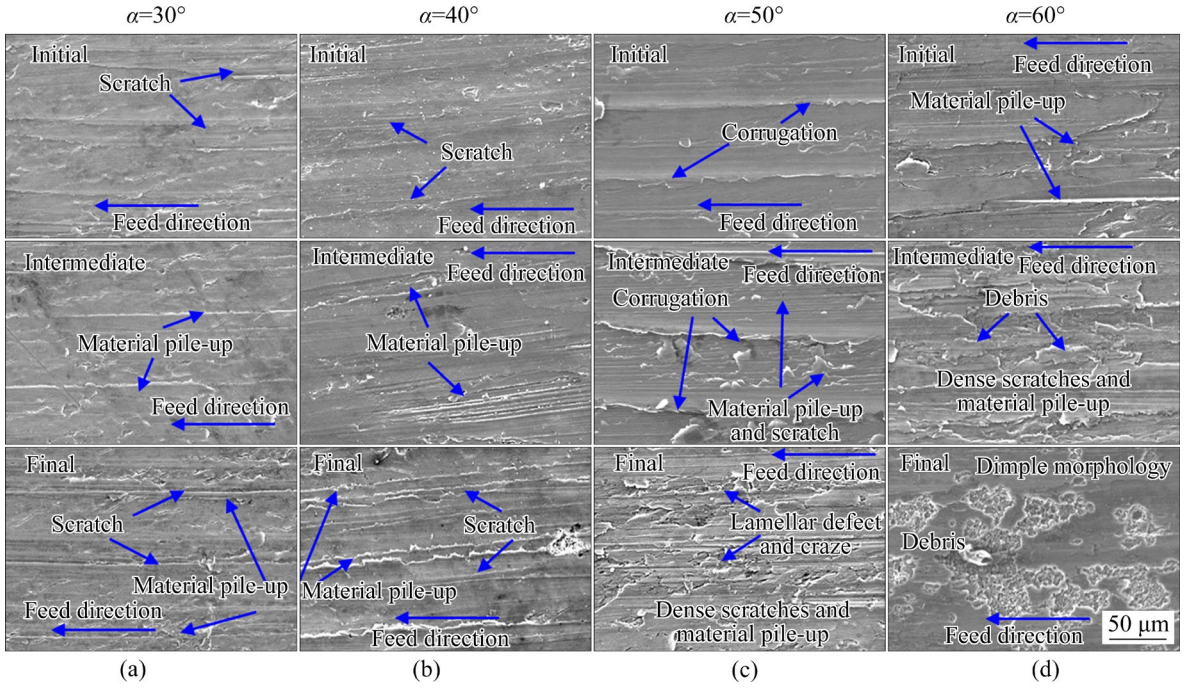

Fig. 8 Surface morphologies of parts throughout forming process at different wall angles: (a) α=30°; (b) α=40°; (c) α=50°; (d) α=60°

Therefore, when $\alpha \leq 40°$, with an increase in α, the strain and newly formed surface area only experience a slight increase, while the surface morphology characteristics remain consistent. This does not reach the threshold for a transition in friction mechanisms, resulting in similar friction coefficients.

On the other hand, when α exceeds 40°, the plastic strain and newly formed surface area significantly increase, as shown in Fig. 5(b). The plastic strain roughening noticeably, and if lubrication is insufficient, the newly formed surface may adhere to the tool, leading to interactions with abrasive wear. This results in an increase in R_a along the feed and meridian directions, as seen in Figs. 6(a) and (b), along with an increase in R_{sk} and a decrease in R_{ku}, as shown in Fig. 7. Consequently, the surface micro-convex peaks only provide a very small supporting area, and their sharp contours increase significantly. The larger newly formed contact area with insufficient lubrication is prone to accelerated adhesive wear. Therefore, after α increases to 50°, the friction mechanism during the initial stages of forming already exhibits micro-cutting action, as the torn edges stack on the surface after multiple extrusions.

As the forming process continues, micro-cutting debris mix into the contact interface, and tool surfaces accumulate built-up edges, continuously micro-cutting the sheet surface. R_a and R_{sk} show an increasing trend, while R_{ku} shows a decreasing trend, as shown in Figs. 6(c) and 7. The phenomenon would result in further cold welding at the peak-to-peak contact interface under high pressure, exerting shear stress on the internal materials of the sheet during relative motion, leading to the formation of microcracks and adhesive wear, as shown in Fig. 8(c), with a noticeable increase in the friction coefficient. Furthermore, as α increases to 60°, the newly formed area continues to increase, leading to the ongoing deterioration of surface parameters, causing an increase in the adhesion area and even the occurrence of scuffing effects. In addition, serious dimple-like defects are formed on the sheet surface, as shown in Fig. 8(d). Consequently, the friction coefficient further increases.

Therefore, the friction characteristics and surface quality are not constant throughout the entire forming process of complex parts with varying wall angles in ISF. For $\alpha \leq 40°$, the friction characteristics and surface quality can be considered to be consistent and relatively optimal. However, for $\alpha > 40°$, the friction characteristics and surface quality gradually decrease as α increases. Additionally, the surface morphology features develop in a direction that is unfavorable for lubrication and friction reduction as the forming process progresses.

4.2 Influence of sheet thickness

As t_0 increases from 0.5 to 1.5 mm, μ rises from 0.1556 to 0.2103. Compared to the friction coefficient at t_0=1 mm, there is a decrease of 18.148% at t_0=0.5 mm, and a decrease of 8.89% at t_0=0.8 mm. However, there is an increase of 3.261% at t_0=1.2 mm, and an increase of 10.626% at t_0=1.5 mm, as depicted in Fig. 9(a). With the increase in t_0, μ demonstrates a consistently increasing trend, signifying a gradual deterioration in the friction conditions. Nonetheless, it is noteworthy that only significant variations in friction conditions occur when there is a considerable disparity in t_0. Thus, this study characterizes the mechanisms behind the changes in friction characteristics for t_0 of 0.5, 1, and 1.5 mm.

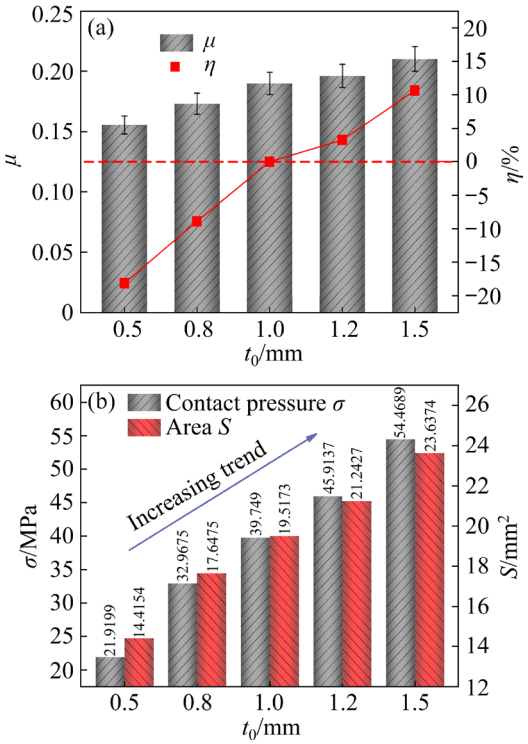

Fig. 9 Friction coefficients and their change rates (a), and contact pressure and area (b) at different sheet thicknesses

As the sheet thickness increases, the plastic strain decreases slightly according to Eq. (5). However, the maximum decrease from 0.5 to 1.5 mm is only 10.473%, indicating that the effect of strain roughening is not significant. In contrast, the corresponding contact pressure increases by 14.491%, and the contact area enlarges by 63.973%, as shown in Fig. 9(b). The higher contact pressure is more likely to squeeze out lubricants at the interface, resulting in an increased proportion of tool hard extruding the sheet surface. Although the friction effect is independent of the nominal contact area, the combined effect of a larger area and higher pressure further causes an increase in the real contact area under the same initial morphology.

Therefore, there is a noticeable increase in R_a due to the direct extruding and plastic flow motion between more micro-asperities as t_o increases, as shown in Figs. 10(a) and (b). At the same time, R_{sk} shifts from negative skewness to positive skewness, and R_{ku} decreases from greater than 3 to less than 3, as shown in Fig. 11. This means that the favorable wedge effect for lubrication and the good supporting surface gradually disappear, and the morphology evolves towards a less favorable direction for the

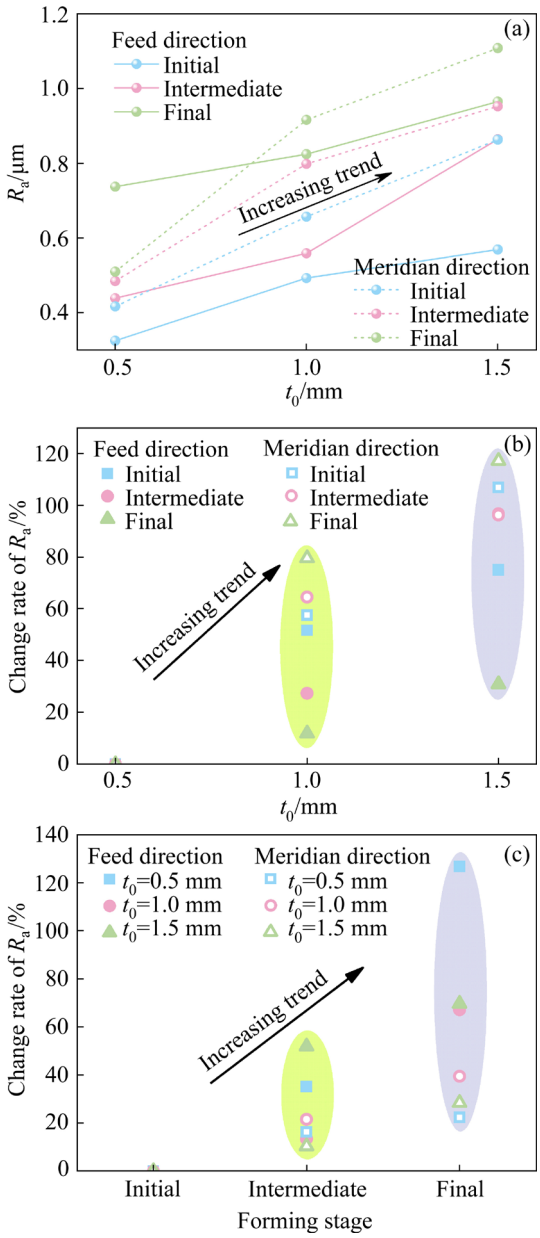

Fig. 10 R_a (a) and change rate of R_a (b) with respect to sheet thickness (b), and change rate of R_a during forming process (c)

lubrication and friction reduction, increasing the real contact area. Therefore, the interface experiences not only plastic extrusion flow, but also deeper micro-plowing and micro-cutting actions at t_0=1.5 mm, leaving deeper scratches and debris on the surface. Plow folds and tearing edges are extruded and piled up on the surface. At the same time, adhesive and shear actions form lamellar debris and defects on the surface. Even when the adhesive strength is large, deep surface cracks can form, resulting in dimple-shaped tearing defects, as shown in Fig. 12(c).

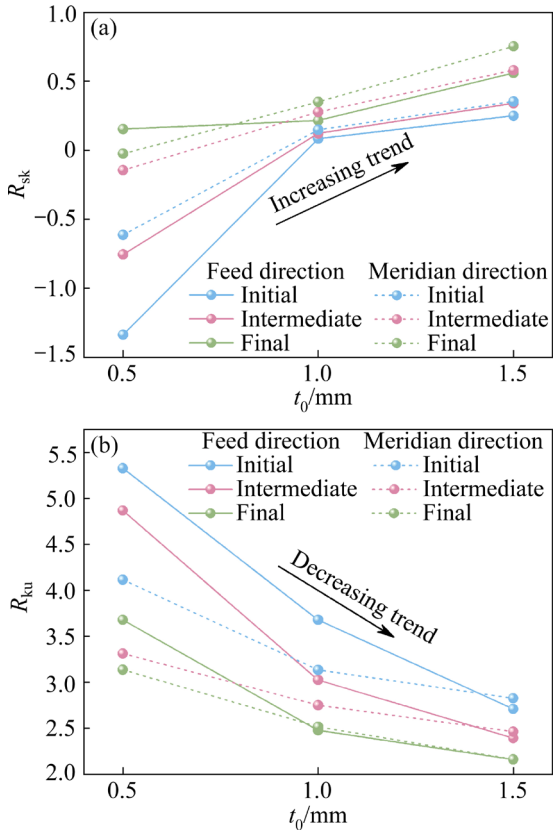

Fig. 11 R_{sk} (a) and R_{ku} (b) throughout forming process at different sheet thicknesses

In contrast, when t_0 is small, such as 0.5 mm, the lubricant can effectively function under favorable morphology and lower pressure conditions, resulting in a smaller real contact area. In addition to the plastic extrusion and shearing motion, only the higher micro-asperities of the tool plow the sheet surface. Upon repeated extrusion, the edges of these scratches pile up on the surface, as shown in Fig. 12(a), exhibiting a reduced friction coefficient. For t_0=1 mm, it is in an intermediate transitional stage between the two mentioned above, as shown in Fig. 12(b), exhibiting friction effects similar to those described in Section 4.1.

Furthermore, it is observed that there is a gradual roughening trend on the surface as the forming process progresses, as depicted in Figs. 10(a) and (c). At the same time, there is an increasing tendency for R_{sk} and a decreasing trend for R_{ku}, as shown in Fig. 11. The surface morphology tends to transition towards a less favorable state for lubrication and friction reduction as the forming process advances. This may be attributed to the inability to remove the debris at the interface during incremental forming of box-shaped

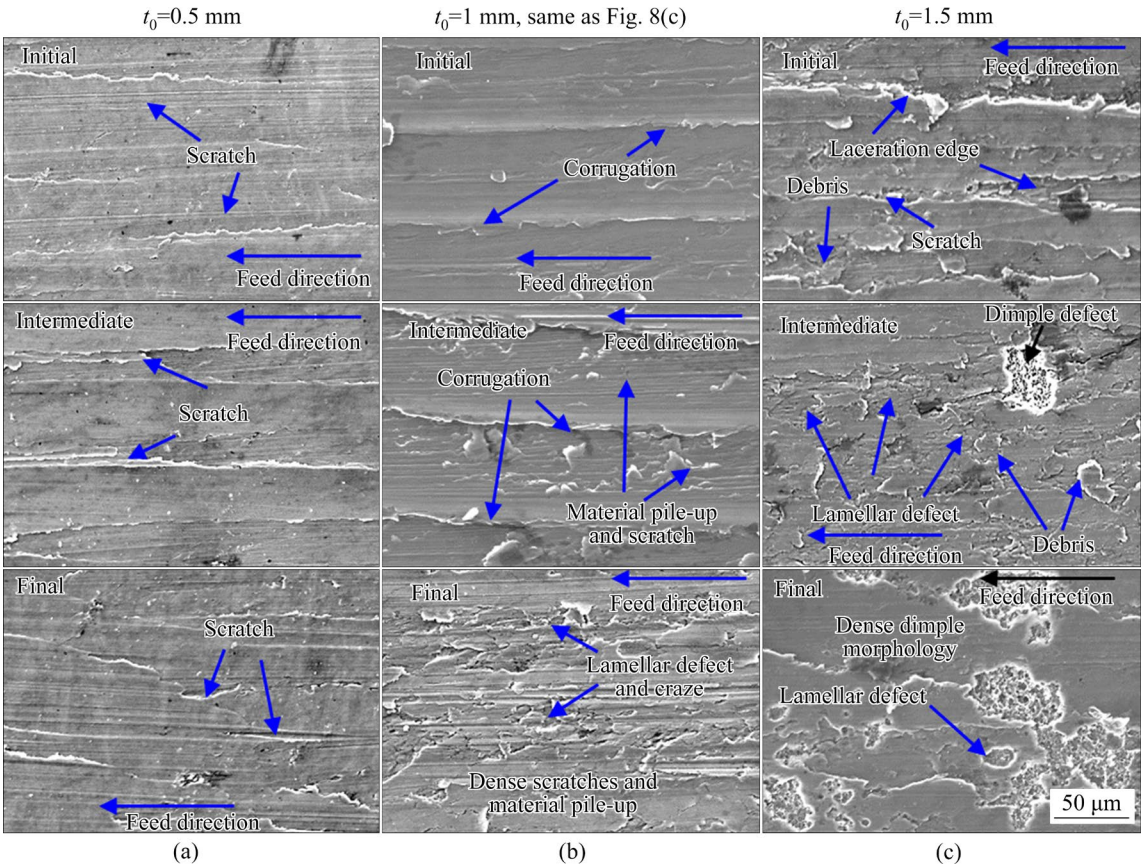

Fig. 12 Surface morphologies of parts throughout forming process with different sheet thicknesses: (a) t_0=0.5 mm; (b) t_0=1 mm; (c) t_0=1.5 mm

parts, where the presence of debris intensifies abrasive wear and leads to deeper scratches on the sheet surface, as evident in Fig. 12(a). When t_0 is larger, the morphology that is less conducive to lubrication increases the adhesive effect, resulting in lamellar defects and even severe dimple-like defects due to scuffing, as illustrated in Fig. 12(c).

Therefore, given the prerequisite of meeting the requirements for structural strength and operational performance of prefabricated parts, the option of utilizing thin sheets for part fabrication arises due to their superior friction characteristics and surface formation quality.

4.3 Influence of tool radius

As R varies from 4 to 10 mm, with μ of 0.2074, 0.1833 and 0.1598, a comparison to the friction coefficient at R=7 mm reveals an increase of 13.148% at R=4 mm, followed by a decrease of 12.821% at R=10 mm, as depicted in Fig. 13. Hence, it is observed that m progressively diminishes with increasing R, thereby presenting a positive enhancement in friction conditions.

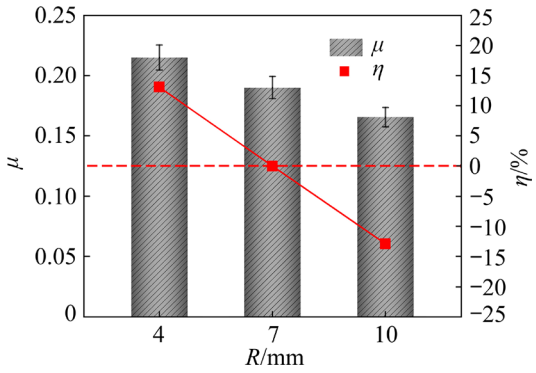

Fig. 13 Friction coefficients and their change rates during ISF with different tool radii

Due to the characteristics of ISF, which involves layer-by-layer extrusion in the feeding direction, there exist corrugated extrusion patterns between the layers, as shown in Fig. 14. As R decreases, the corrugation height increases, and the surface morphological parameters tend towards roughness, which is unfavorable for lubrication.

It can be observed that a slight decrease occurs in the plastic strain as R decreases according to Eq. (5). However, the maximum reduction from R=

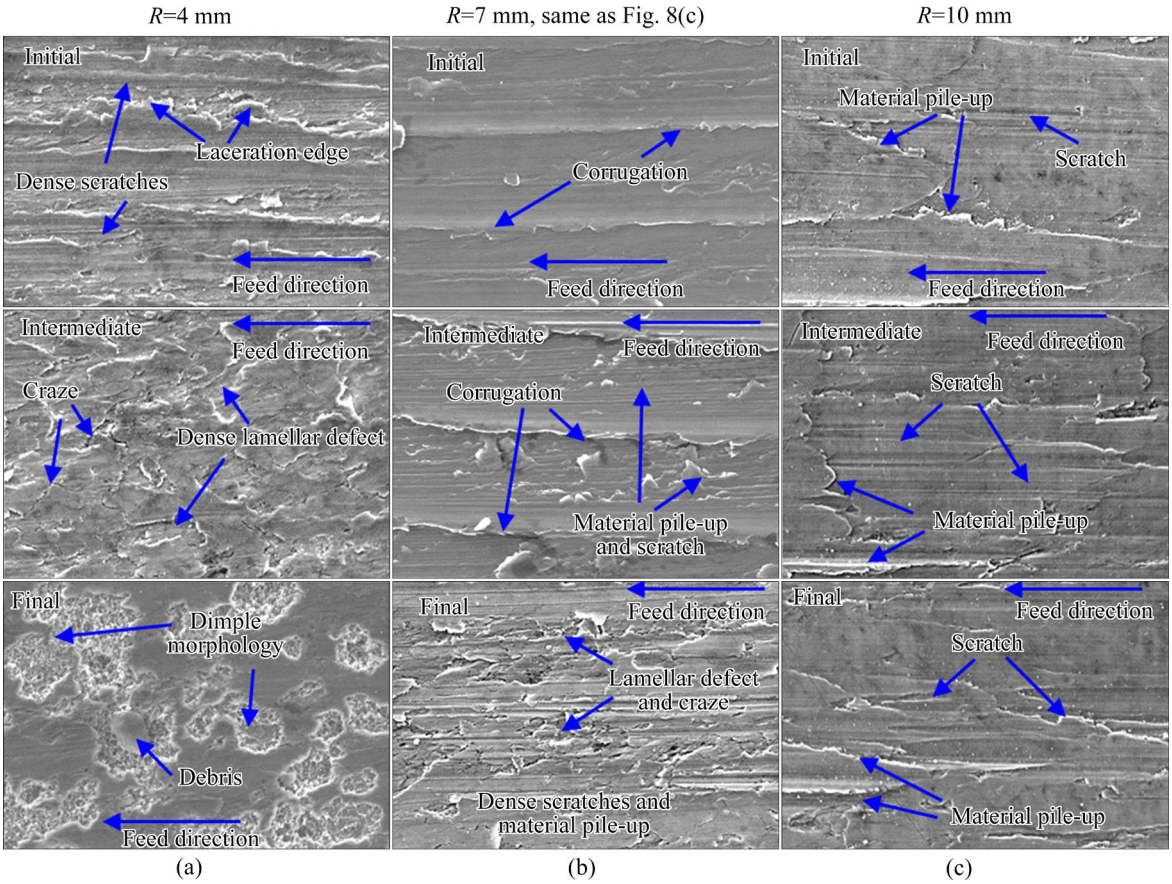

Fig. 14 Surface morphologies of parts formed by different tool radii throughout entire forming process: (a) R=4 mm; (b) R=7 mm; (c) R=10 mm

10 mm to R= 4 mm is only 11.123%, indicating that the morphological parameter change resulting from strain is not significant. On the other hand, the contact pressure increases by 108.834%. The higher pressure causes the lubricant to be squeezed out from the interface, resulting in greater direct solid contact between the tool and the sheet. This leads to increased plowing depth. Hence, the aforementioned combined effects result in surface roughening when smaller radius tools are employed, as illustrated in Figs. 15(a) and (b). Additionally, the surface morphology exhibits a positive R_{sk} that is unfavorable for lubrication, as well as an increased R_{ku}, which contributes to a larger real contact area, as shown in Fig. 16.

Thus, there is closer contact between the tool and the sheet during the use of smaller radius tools, resulting in more and deeper plowing scratches. Simultaneously, the corrugation material from extrusion, the edge material from plowing, and the torn edge material from micro-cutting form material stacks through repeated extrusion. Under higher loads, the cold welding effect resulting from direct extrusion contact leads to the formation of cracks during relative tangential motion. With further relative movement, these cracks tear and form lamellar-like defects, resulting in lamellar-like debris as depicted in Figs. 14(a) and (b). Furthermore, with the increasing presence of debris at the interface, the depth of the cracks intensifies. Under the traction of shearing stress, deeper-layer tearing occurs, leaving behind dimple-like tear defects on the surface, as shown in the final stage of the forming process in Fig. 14(a).

On the contrary, the contact pressure is reduced when larger radius tools are used. Additionally, the favorable morphological R_{sk} and R_{ku} contribute to capturing lubricants at the interface, isolating direct contact between the tool and the sheet. This condition promotes the effective action of the lubricant, resulting in a relatively small real contact area. The surface exhibits only plow marks, material piles up from plowing, and plastic flow traces, as depicted in Fig. 14(c). Therefore, larger tool radii correspond to lower friction coefficients.

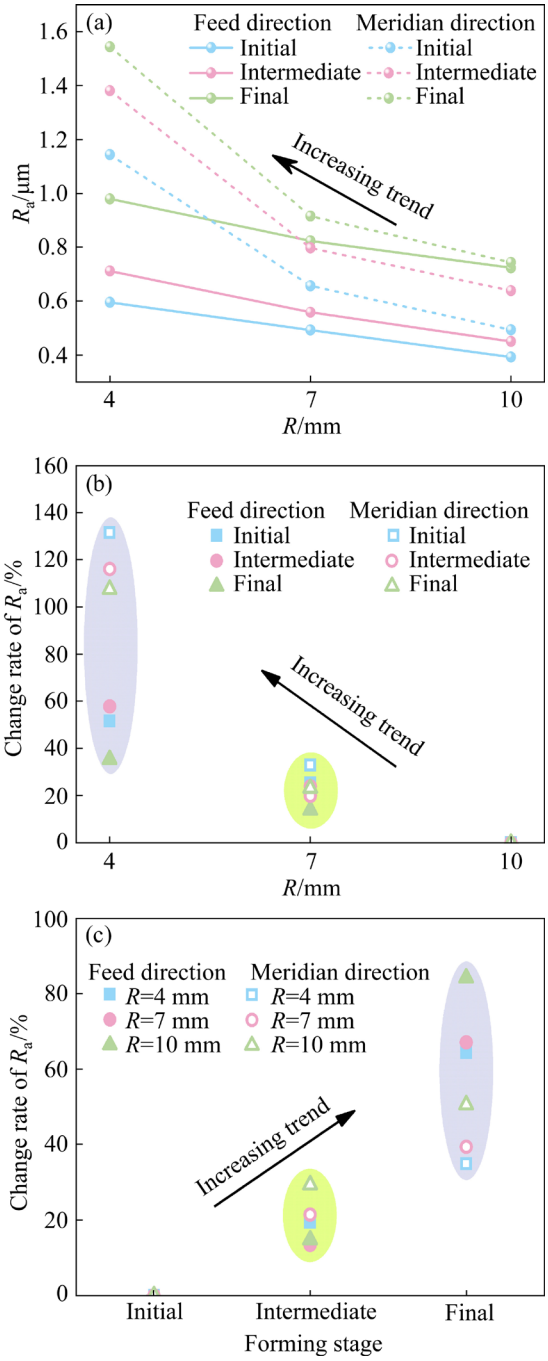

Fig. 15 R_a (a) and change rate of R_a (b) with respect to tool radius, and change rate of R_a with respect to forming process (c)

Furthermore, the surface morphology formed with tools of the same size also tends to gradually roughen as the forming process progresses, as illustrated in Figs. 15(a) and (c). R_{sk} and R_{ku} also develop in a direction that hinders the effectiveness of lubricants and increases the contact area, as shown in Fig. 16. Therefore, the plowing effect intensifies as the forming process continues, leading to an increase in adhesion and further reducing the

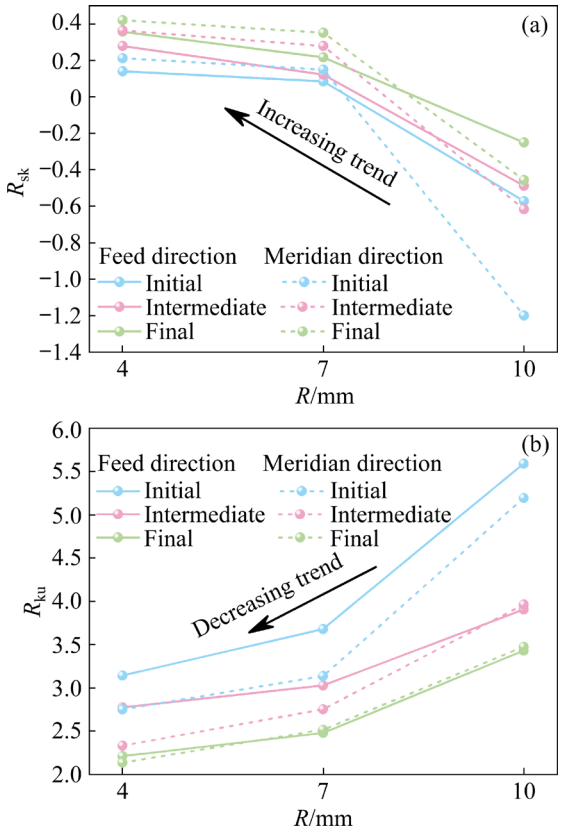

Fig. 16 R_{sk} (a) and R_{ku} (b) throughout forming process at different tool radius

surface quality, as depicted in Fig. 14. The main cause of this phenomenon, specifically the increased presence of debris at the interface, has been explained in Sections 4.1 and 4.2.

Therefore, while meeting the minimum bending radius requirement for the prefabricated parts, it can be considered to choose larger-sized tools for forming to improve the friction conditions and the surface quality.

4.4 Influence of plane curve feature

Compared to pyramid parts with different wall angles, the maximum change rate of the friction coefficient for cone parts is only 4.885%, occurring at α=30°. Similarly, the maximum change rate of the friction coefficient for elliptical cone parts is only 4.686%, also occurring at α=30°, as shown in Fig. 17(a). Compared to pyramid parts with different sheet thicknesses, the maximum change rate of the friction coefficient for cone parts is only −3.577%, occurring at t_0=1 mm. Likewise, the maximum change rate of the friction coefficient for elliptical cone parts is only −3.104%, occurring at t_0=1 mm, as shown in Fig. 17(b).

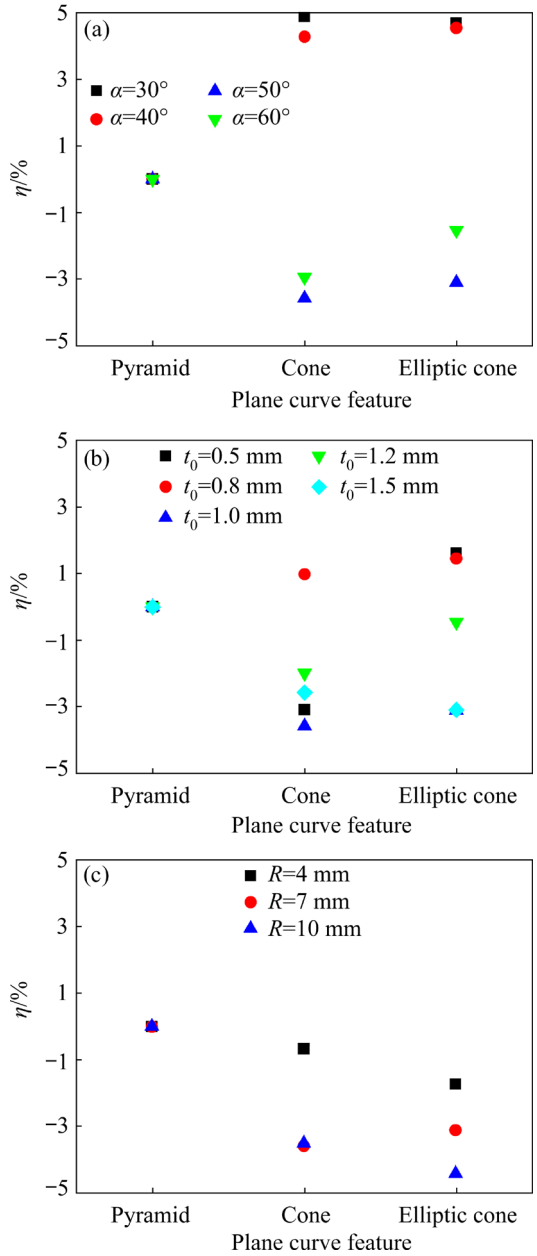

Fig. 17 Change rate in friction coefficient among parts with different plane curve features: (a) Wall angle; (b) Sheet thickness; (c) Tool radius

Furthermore, when compared to pyramid parts formed using tools with different radii, the maximum change rate of the friction coefficient for cone parts is only −3.577%, occurring at R=7 mm. Similarly, the maximum change rate of the friction coefficient for elliptical cone parts is only −4.408%, happening at R=10 mm, as shown in Fig. 17(c). Within a wide range of geometric configuration parameter variations, where only the plane curve features of the part differ, the change in friction coefficient remains below 5%. The insignificant changes would not cause significant alterations in the process of ISF, and therefore, can be disregarded.

The main factors affecting the friction system in ISF are shown in Table 3, which include material and its processing state, initial surface morphology, deformation characteristics, process parameters, lubrication conditions, environmental temperature, forming force, and contact area. Any variation in these factors would cause a change in the friction coefficient. However, when other process parameters are the same and only parts with different plane curve features are formed, the material and processing state of the tool and the sheet, as well as the parameters of the initial surface morphology, remain consistent as described in Section 3.1. They are all in a plane strain state, with the same strain [4]. Process parameters and lubrication conditions are also kept consistent as described in Section 3.2. The experiments are conducted at room temperature. It can be determined that the contact area is independent of the part's plane curve features according to Eq. (2).

Table 3 Main factors influencing friction system

Factor	Pyramid, cone and elliptical cone
Material and its processing state	In line with consistency, as stated in Section 3.1
Initial surface morphology	In line with consistency, as stated in Section 3.1
Deformation characteristics	Plane strain state
Process parameters	In line with consistency, as stated in Section 3.2
Lubrication condition	L-HM46 oil
Environmental temperature	Room temperature
Forming force	Rate of change does not exceed ±3%, as shown in Fig. 18
Contact area	Independent of the characteristics of the plane curve features

The forming forces for parts with different plane curve features are similar, with deviations smaller than ±3%, as shown in Fig. 18. For 30°≤α≤60°, the maximum variation is only 1.630%; for 0.5 mm≤t_0≤1.5 mm, the maximum variation is only −2.847%; for 4 mm≤R≤10 mm, the maximum variation is only −2.404%. The minimal deviations may originate from instrument drift, external vibrations, etc, and can be ignored. The consistency

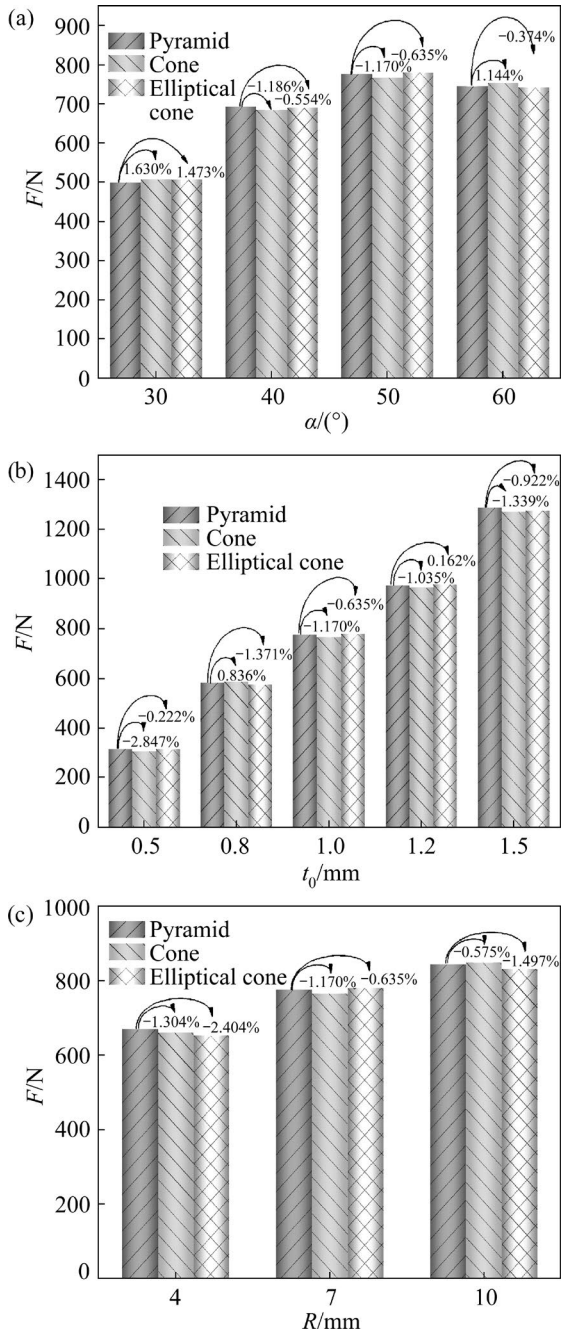

Fig. 18 Forming forces at various geometric configuration parameters: (a) Wall angle; (b) Sheet thickness; (c) Tool radius

of various important factors influencing the friction system establishes the basis for similar friction characteristics in forming parts with different plane curve features.

This work only describes the study of the friction characteristics when forming pyramid, cone, and elliptical cone parts under specific geometric parameters. The research methodology for studying the friction characteristics between parts with different plane curve features under other geometric parameters is similar and would not be elaborated.

R_a remains relatively consistent throughout the entire forming process of parts with different plane curve features, with variations of less than 10%. Moreover, there is a tendency for gradual roughening as the forming process progresses, as shown in Fig. 19. R_{sk} gradually increases, while R_{ku} gradually decreases during the forming process, indicating the evolving surface towards a less favorable lubrication direction, as depicted in Fig. 20.

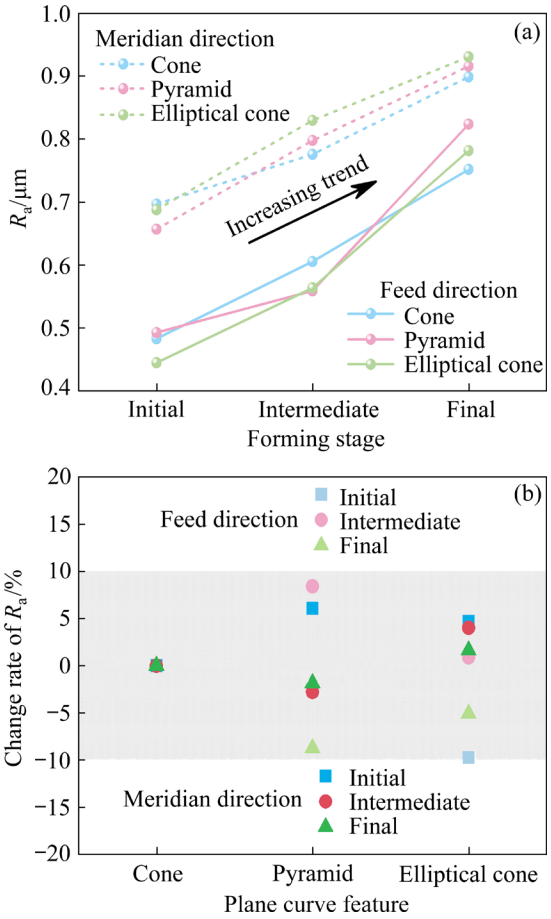

Fig. 19 R_a (a), and change rate of R_a (b) among different plane curve feature parts

Therefore, the friction mechanism in the forming initial stages for various plane curve features parts primarily involves micro-plowing, micro-cutting action, and material pile-up caused by plastic extrusion flow and combined action. As the forming process continues, more debris enters the interface, leading to a gradual surface roughening for parts with different plane curve features, favoring reduced lubrication and increased contact area. This leads to an increase in plowing and

cutting depths, a higher proportion of adhesion, and the formation of cracks and lamellar defects caused by shear stress induced by plastic material flow, as illustrated in Fig. 21.

In summary, the friction mechanism remains the same when only the plane curve feature varies, resulting in consistent friction coefficients. However, there may be a slight worsening trend due to the increased generation of debris during the forming process.

4.5 Friction mechanism

Based on the analysis of the friction characteristics in Sections 4.1−4.4, it is observed that there is no significant strain roughening when $\alpha \leq 40°$, a small newly formed area in the forming of thin sheets with t_0=0.5 mm, and a smaller contact pressure when a large tool radius of R=10 mm. This results in a better surface morphology, which is beneficial for capturing lubricant and exerting lubricating effects. Due to the smaller direct contact

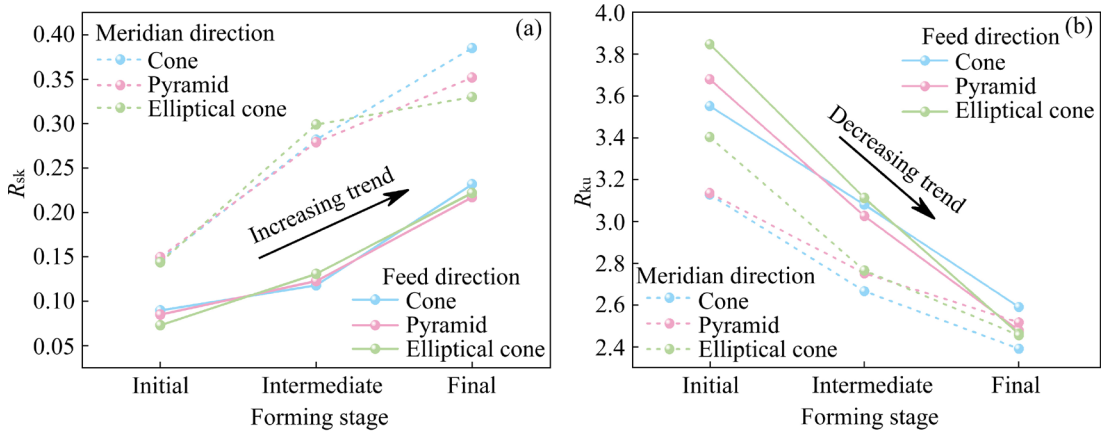

Fig. 20 R_{sk} (a) and R_{ku} (b) throughout forming process at different plane curve feature parts

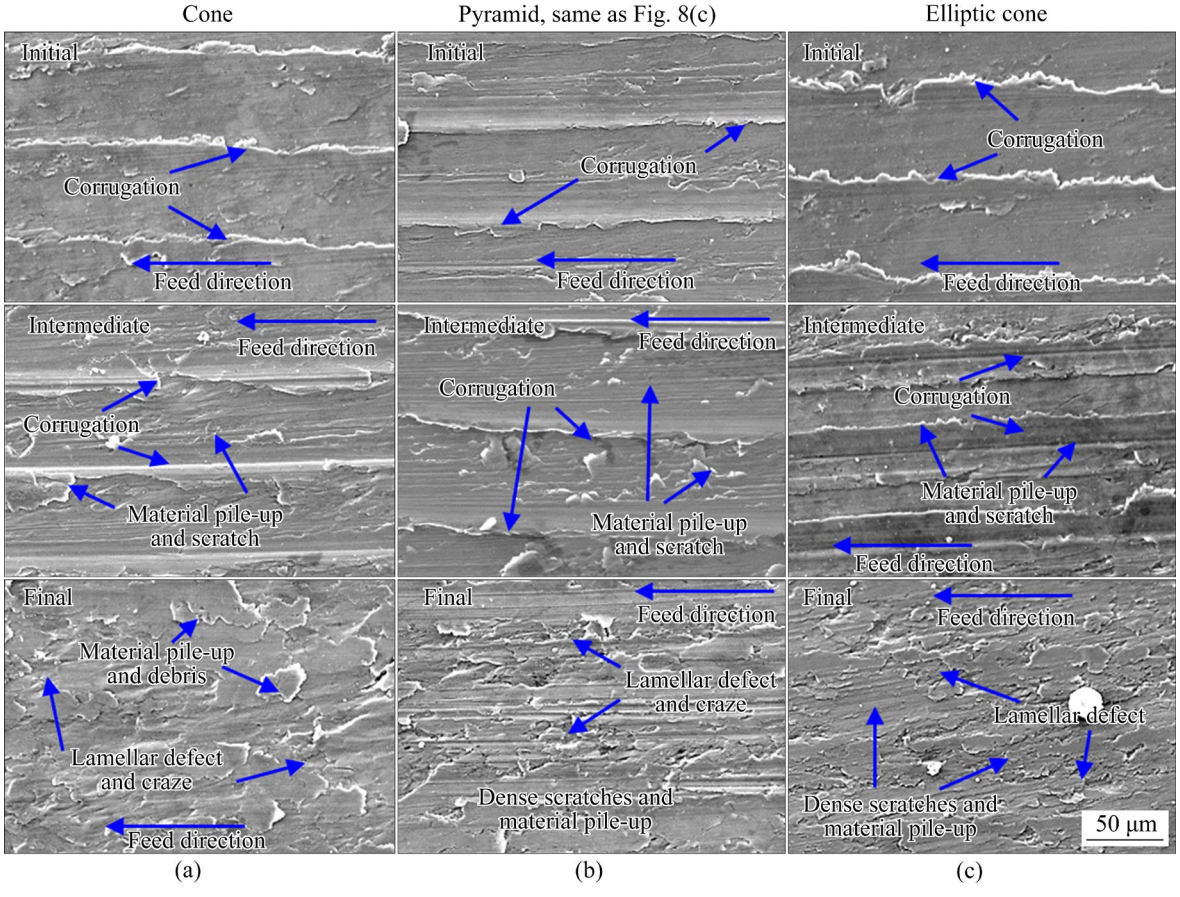

Fig. 21 Surface morphologies of different plane curve feature parts: (a) Cone; (b) Pyramid; (c) Elliptical cone

area, the dominant mechanisms are micro-plowing and plastic extrusion, causing material pile-up after the edge of the plowed wrinkle and plastic material flow are extruded. Furthermore, the lubricant plays a certain lubricating role, leading to a mixed lubrication state and exhibiting a smaller friction coefficient. This results in a relatively better surface quality, as shown in Fig. 22(a).

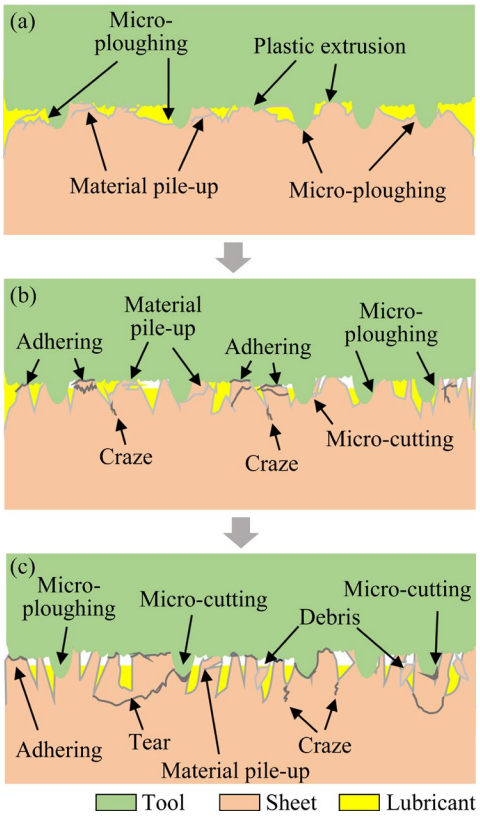

Fig. 22 Evolution of friction mechanisms

The plastic strain roughening becomes prominent and the newly formed area continues to increase when α increases to 50°. The contact pressure and area are large when t_0 is 1 mm. The contact pressure experiences a significant increase when R decreases to 7 mm. As a result, the sheet surface becomes rougher, which is unfavorable for lubrication. The increase in direct contact area inhibits the effectiveness of the lubricant, leading to a higher proportion of dry friction in the mixed lubrication. Therefore, the interface also exhibits significant micro-cutting and adhesion in addition to micro-plowing and plastic extrusion. The edges that are torn during micro-cutting experience repeated extrusion, which results in the formation of pronounced material pile-up. In the region of adhesion, the relative motion causes the shallow surface layer of the soft sheet to peel off, forming a lamellar defect. Simultaneously, the shear stress leads to the movement of the adhered point on the soft sheet surface, causing stress concentration at the groove and forming cracks gradually. This results in a higher friction coefficient, forming a surface with larger roughness and unfavorable for lubrication, indicating relatively poor surface quality, as shown in Fig. 22(b).

As α increases to 60°, t_0 increases to 1.5 mm, and R decreases to 4 mm, sheet surface roughening becomes more pronounced. The lubricant is further squeezed out of the interface, resulting in a continuous increase in the direct contact area and a large proportion of the adhesive area. Hence, the interface experiences not only plastic extrusion, micro-plowing, micro-cutting, and adhesive wear, but also deeper dimple-like tearing defects due to local scuffing. Consequently, higher friction coefficients are exhibited during this stage, resulting in poorer surface quality of the formed part, as depicted in Fig. 22(c).

5 Conclusions

(1) For $\alpha \leq 40°$, minimal plastic strain roughening and small newly formed surface area are observed. When forming a thin sheet with t_0= 0.5 mm, small contact pressure and area are maintained. A larger tool (R=10 mm) results in lower contact pressure. These factors contribute to surface morphology favorable for lubrication and support. The interface operates in a mixed lubrication state, featuring micro-plowing and plastic extrusion flow, resulting in a low friction coefficient.

(2) After α surpasses 40°, notable plastic strain roughening causes persistent enlargement of inadequately lubricated newly formed surfaces. At t_0=1 mm or R=7 mm, contact pressure significantly increases, adversely affecting surface morphology for lubrication and support. Increased direct dry friction contact shifts primary friction mechanisms to micro-plowing and adhesive wear, elevating the friction coefficient. Even at α=60°, or t_0=1.5 mm, or R=4 mm, localized scuffing forms dimple-like tearing defects.

(3) Plane curve features do not affect the interfacial friction mechanism, because the main factors affecting the friction system remain

consistent, and the surface morphology characteristics remain similar throughout the forming process. Despite geometric configuration parameters, abrasive debris cannot be effectively removed from the interface during forming process, leading to an increased proportion of abrasive wear. Consequently, surface morphology evolves unfavorably for lubrication and friction reduction.

CRediT authorship contribution statement

Guang-can YANG: Conceptualization, Methodology, Investigation, Data curation, Formal analysis, Writing − Original draft; **Da-wei ZHANG:** Conceptualization, Methodology, Writing − Reviewing and editing; **Chong TIAN:** Sample preparation, Measurements; **Sheng-dun ZHAO:** Supervision.

Declaration of competing interest

The authors declare that they have no known competing financial interests or personal relationships that could have appeared to influence the work reported in this paper.

Acknowledgments

The authors would like to gratefully acknowledge the support of the Key Research and Development Program of Shaanxi Province, China (No. 2021GXLH-Z-049).

References

[1] AL-GHAMD K A, HUSSAIN G. Bulging in incremental sheet forming of cold bonded multi-layered Cu clad sheet: Influence of forming conditions and bending [J].Transactions of Nonferrous Metals Society of China, 2019, 29: 112−122.

[2] HUSSAIN G, ILYAS M, LEMOPI ISIDORE B B, KHAN W A. Mechanical properties and microstructure evolution in incremental forming of AA5754 and AA6061 aluminum alloys [J]. Transactions of Nonferrous Metals Society of China, 2020, 30: 51−64.

[3] HIRSCH J. Recent development in aluminium for automotive applications [J]. Transactions of Nonferrous Metals Society of China, 2014, 24: 1995−2002.

[4] SILVA M B, SKJOEDT M, MARTINS P A F, BAY N. Revisiting the fundamentals of single point incremental forming by means of membrane analysis [J]. International Journal of Machine Tools and Manufacture, 2008, 48: 73−83.

[5] BEHERA A K, de SOUSA R A, INGARAO G, OLEKSIK V. Single point incremental forming: An assessment of the progress and technology trends from 2005 to 2015 [J]. Journal of Manufacturing Processes, 2017, 27: 37−62.

[6] HOSSEINI KORDKHEILI S A, ASHRAFIAN M M, TOOZANDEHJANI H. A rate-dependent constitutive equation for 5052 aluminum diaphragms [J]. Materials & Design, 2014, 60: 13−20.

[7] ZHANG Da-wei, YANG Guang-can, ZHAO Sheng-dun. Frictional behavior during cold ring compression process of aluminum alloy 5052 [J]. Chinese Journal of Aeronautics, 2021, 34: 47−64.

[8] SIGVANT M, PILTHAMMAR J, HOL J, WIEBENGA J H, CHEZAN T, CARLEER B, VAN DEN BOOGAARD T. Friction in sheet metal forming: Influence of surface roughness and strain rate on sheet metal forming simulation results [J]. Procedia Manufacturing, 2019, 29: 512−519.

[9] BAMBACH M, HIRT G, JUNK S. Modelling and experimental evaluation of the incremental CNC sheet metal forming process [C]// Proc 7th COMPLAS Congress. Barcelona, PA: COMPLAS, 2003: 7−10.

[10] ALLWOOD J M, SHOULER D R, TEKKAYA A E. The increased forming limits of incremental sheet forming processes [J]. Key Engineering Materials, 2007, 344: 621−628.

[11] JACKSON K P, ALLWOOD J M, LANDERT M. Incremental forming of sandwich panels [J]. Journal of Materials Processing Technology, 2008, 204: 290−303.

[12] CHANG Zhi-dong, CHEN Jun. Mechanism of the twisting in incremental sheet forming process [J]. Journal of Materials Processing Technology, 2020, 276: 116396.

[13] YANG Zhi-yun, CHEN Fei. Mechanism of twist in incremental sheet forming of thermoplastic polymer [J]. Materials & Design, 2020, 195: 108997.

[14] ISEKI H. An approximate deformation analysis and FEM analysis for the incremental bulging of sheet metal using a spherical roller [J]. Journal of Materials Processing Technology, 2001, 111(1): 150−154.

[15] SHIM M S, PARK J J. The formability of aluminum sheet in incremental forming [J]. Journal of Materials Processing Technology, 2001, 113(1): 654−658.

[16] LU Bin, FANG Yong-yong, XU Dong-kai, CHEN Jun, OU H, MOSER N H, CAO Jian. Mechanism investigation of friction-related effects in single point incremental forming using a developed oblique roller-ball tool [J]. International Journal of Machine Tools and Manufacture, 2014, 85: 14−29.

[17] BHATTACHARYA A, SINGH S, MANEESH K, VENKATA REDDY N, CAO J. Formability and surface finish studies in single point incremental forming [J]. Journal of Manufacturing Science and Engineering, 2011, 133(6): 061020.

[18] KUMAR A, GULATI V, KUMAR P. Investigation of surface roughness in incremental sheet forming [J]. Procedia Computer Science, 2018, 133: 1014−1020.

[19] KUMAR A, GULATI V. Experimental investigation and optimization of surface roughness in negative incremental forming [J]. Measurement, 2019, 131: 419−430.

[20] DURANTE M, FORMISANO A, LANGELLA A. Comparison between analytical and experimental roughness values of components created by incremental forming [J]. Journal of Materials Processing Technology, 2010, 210(14): 1934−1941.

[21] MOHANTY S, REGALLA S P, RAO Y V D. Influence of process parameters on surface roughness and forming time of Al-1100 sheet in incremental sheet metal forming [J]. Journal of Mechanical Engineering and Sciences, 2019, 13(2): 4911−4927.

[22] KUMAR V, KUMAR R. Investigation of surface roughness in incremental sheet forming of AA 2014-T6 using Taguchi's method [J]. Journal of Physics: Conference Series, 2020, 1519(1): 012009.
[23] KURRA S, HR N, REGALLA S, GUPTA A K. Parametric study and multi-objective optimization in single-point incremental forming of extra deep drawing steel sheets [J]. Proceedings of the Institution of Mechanical Engineers, Part B: Journal of Engineering Manufacture, 2016, 230(5): 825−837.
[24] LIU Zhao-bing, LIU Sheng, LI Yan-le, MEEHAN P A. Modeling and optimization of surface roughness in incremental sheet forming using a multi-objective function [J]. Materials and Manufacturing Processes, 2014, 29(7): 808−818.
[25] ZHANG Qing-lai, XIAO Fu-gui, GUO Hai-ling, LI Chang-sheng, GAO Lin, GUO Xing-wu, HAN Wei-dong, BONDAREV A B. Warm negative incremental forming of magnesium alloy AZ31 Sheet: New lubricating method [J]. Journal of Materials Processing Technology, 2010, 210(2): 323−329.
[26] XU Chang-xu, LI Yan-le, WANG Zi-jian, CHENG Zi-nan, LIU Fu-yuan. The influence of self-lubricating coating during incremental sheet forming of TA1 sheet [J]. The International Journal of Advanced Manufacturing Technology, 2020, 110: 2465−2477.
[27] DIABB J, RODRIGUEZ C A, MAMIDI N, SANDOVAL J A, TAHA-TIJERINA J, MARTINEZ-ROMERO O, ELIAS-ZUNIGA A. Study of lubrication and wear in single point incremental sheet forming (SPIF) process using vegetable oil nanolubricants [J]. Wear, 2017, 376/377(part A): 777−785.
[28] DIABB Z J M, MARTINEZ-ROMERO O, ELIAS -ZUNIGA A, LEIJA GUTIERREZ H M, ESTRADA-DE LA VEGA A, TAHA-TIJERINA J. Study of friction and wear effects in aluminum parts manufactured via single point incremental forming process using petroleum and vegetable oil-based lubricants [J]. Materials, 2021, 14(14): 3973.
[29] ŞEN N, ŞIRIN Ş, KIVAK T, CIVEK T, SEÇGIN Ö. A new lubrication approach in the SPIF process: Evaluation of the applicability and tribological performance of MQL [J]. Tribology International, 2022, 171: 107546.
[30] LI Xiao-qiang, HAN Kai, SONG Xu, WANG Hai-bo, LI Dong-sheng, LI Yan-le, LI Qing. Experimental and numerical investigation on surface quality for two-point incremental sheet forming with interpolator [J]. Chinese Journal of Aeronautics, 2020, 33(10): 2794−2806.
[31] LI Cai-ling, ZHAO Chang-xi, LI Ji-xia. Analysis of aerospace application prospect of NC incremental forming technology [J]. Science and Technology Innovation Herald, 2010, 7(21): 95−96. (in Chinese)
[32] MO Jian-hua, HAN Fei. State of the arts and latest research on incremental sheet NC forming technology [J]. China Mechanical Engineering, 2008, 19(4): 491−497. (in Chinese)
[33] LU B, OU H, SHI S Q, LONG H, CHEN J. Titanium based cranial reconstruction using incremental sheet forming [J]. International Journal of Material Forming, 2016, 9(3): 361−370.
[34] AMBROGIO G, NAPOLI L D, FILICE L, GAGLIARDI F, MUZZUPAPPA M. Application of Incremental Forming process for high customised medical product manufacturing [J]. Journal of Materials Processing Technology, 2005, 162(10): 156−162.
[35] CHANG Zhi-dong, LI Ming, CHEN Jun. Analytical modeling and experimental validation of the forming force in several typical incremental sheet forming processes [J]. International Journal of Machine Tools & Manufacture, 2019, 140: 62−76.
[36] FANG Yong-yong, LU Bin, CHEN Jun, XU Dong-kai, OU H. Analytical and experimental investigations on deformation mechanism and fracture behavior in single point incremental forming [J]. Journal of Materials Processing Technology, 2014, 214: 1503−1515.
[37] WEN Shi-zhu, HUANG Ping, TIAN Yu, MA Li-ran. Principles of tribology [M]. 5th ed. Beijing: Tsinghua University Press, 2018. (in Chinese)

几何构型对 AA5052 板材渐进成形过程摩擦特性的影响

杨光灿，张大伟，田 冲，赵升吨

西安交通大学 机械工程学院，西安 710049

摘 要：将表面形貌及其特征参数与塑性应变、接触压强及面积结合，分析几何构型对 AA5052 板材渐进成形过程摩擦特性的影响。结果表明：当壁角≤40°、厚度 0.5 mm 的薄板、10 mm 的大工具半径成形时，表面形貌有利于润滑和支撑，界面发生微犁沟和塑性挤压作用，表现出较小的摩擦因数。当壁角大于 40°时，应变粗糙化显著，导致新生表面未及时被润滑，而增加板厚和减小工具半径会增大接触压强。上述作用会触发微切削和黏着作用，甚至发生局部咬死形成韧窝撕裂，表现出更高的摩擦因数。零件的平面曲线特征不会影响界面的摩擦作用机制。此外，随着成形过程的进行，磨粒磨损加剧，表面形貌向着不利于润滑减摩方向演变。

关键词：AA5052 板材；渐进板材成形；几何构型；表面形貌特征；摩擦机制

(Edited by Xiang-qun LI)